Journal of Food Engineering 250 (2019) 9–17

Contents lists available at ScienceDirect

Journal of Food Engineering

journal homepage: www.elsevier.com/locate/jfoodeng

Modeling of convective drying of cornstarch-alginate gel slabs

Marco A.V. Silva Júnior[a], José A. Rabi[b], Rogers Ribeiro[a], Gustavo C. Dacanal[a,*]

[a] Department of Food Engineering, Faculty of Animal Science and Food Engineering, University of São Paulo, FZEA-USP, 13635-900, Pirassununga, SP, Brazil
[b] Department of Biosystems Engineering, Faculty of Animal Science and Food Engineering, University of São Paulo, FZEA-USP, 13635-900, Pirassununga, SP, Brazil

ARTICLE INFO

Keywords:
Drying
Cornstarch
Alginate
Shrinkage
Gelatinization
Finite elements method

ABSTRACT

This work aimed at developing numerical models to predict the moisture and size of slices of gels containing gelatinized or native cornstarch and calcium alginate, during convective drying. The coupling of mass transfer and shrinkage simulated the drying kinetics with evaluation of effective mass diffusivity. Drying of gels containing 34% wb cornstarch (GC90 and RC90 samples) were well fitted by the analytical solution of Fick's second law, with R^2 of 0.963–0.998. The numerical model developed in finite element method via COMSOL Multiphysics better described the drying of gels formulated with 5.4% wb of cornstarch (GC50 and RC50 samples), yielding R^2 of 0.958–0.992. Shrinkage was estimated by the molar flux of water and simulated by the Arbitrary Lagrangian-Eulerian (ALE) method. The shrinkage term modified the drying rate profiles and a pseudo-constant rate period was observed. The developed model can be applied in drying studies of gels or foodstuffs with high shrinkage ratio.

1. Introduction

Natural edible polymers (e.g. starch, alginate, chitosan and gelatin) can be used to formulate gels with high water absorption capacity. The gels are structured by molecular binding mechanisms (e.g. retrogradation and ionic gelling) and are able to retain active compounds in their polymer matrix. The production of microcapsules of gels with either probiotics, bioactive, antioxidants or other ingredients to be preserved during storage is a growing technology in food and pharmaceutical areas. The microcapsules of gels are usually obtained from aqueous suspensions containing natural polymers (e.g. alginate, proteins, gelatin and polysaccharides) while a carrier material is used as filler (e.g. starch, lactose, maltodextrin, proteins and fibers) (Balanč et al., 2016; Flores-andrade et al., 2015; Rojas-Moreno et al., 2018; Us-Medina et al., 2018; Yu et al., 2017).

Drying of gels or suspensions of natural polymers can be accomplished via spray drying, lyophilization, fluidized bed and convective drying technologies. Operational parameters such as vapor pressure, temperature, air velocity, and equilibrium moisture need to be monitored so as to produce a dry solid without degradation of active compounds. Dry solids are easily handling, presenting lower storage volumes and reduced transportation costs (Mujumdar, 2006).

Convective drying of foods consists of moisture removal by simultaneous heat and mass transfer while considering temperature-dependent mass diffusivity and shrinkage (Khan et al., 2017; Kumar et al., 2015). Heat is transferred from hot drying air stream to wet solid. Vaporization occurs at wet bulb temperature on wet solid surface and heat transfer is due to convection and conduction. Thermal radiation may also be relevant when an external heat source is applied (Castro et al., 2018).

Volume reduction is proportional to moisture removal and it can be represented by a linear relationship between shrinkage and moisture on a dry basis (Raghavan et al., 1995). Coupling of Arbitrary Lagrange-Eulerian (ALE) method has been used to model the geometry deformation, thus better describing drying profiles (Ajani et al., 2017). Shrinkage can change the mass (moisture) flux on solid surface, thus modifying the drying rate (Valentas et al., 1997).

Materials subjected to different drying conditions may present changes in their microstructure and in retention of actives compounds. For example, effective mass diffusivity was obtained from antioxidant release assays of chitosan edible films in distilled water (Thakhiew et al., 2011).

Due to coupling of aforesaid transport and physical phenomena, the comprehensive knowledge of convective drying of food products becomes complex and numerical tools are required. The finite elements method (FEM) is suitable to discretize governing differential equations coupling a number of physical phenomena under different geometries.

By considering mass, heat and momentum transport in the convective drying of plums with volumetric shrinkage coupling, the FEM model proposed in Sabarez (2012) was able to predict temperature,

* Corresponding author.
E-mail address: gdacanal@usp.br (G.C. Dacanal).

https://doi.org/10.1016/j.jfoodeng.2019.01.015
Received 10 September 2018; Received in revised form 26 December 2018; Accepted 24 January 2019
Available online 25 January 2019

humidity and ingredients concentration profiles within solids. In Perussello et al. (2014), sucralose concentration in Yacon root slices was simulated via FEM under osmotic dehydration and convective drying. Bearing in mind the effect of size and geometric shape in final food quality, FEM was applied in Defraeye (2017) to simulate the drying of cut apples in the form of cubes, rectangles, circles and semicircles.

Among FEM-based numerical simulators, COMSOL Multiphisics® arises as powerful off-the-shelf software for engineering applications. The convective drying with intermittent microwaves was studied in Kumar et al. (2016) so that temperature and humidity inner profiles as well as vapor pressure profiles on solids surface were numerically simulated via aforesaid FEM software. However, numerical simulations must be validated against experimental data and values of effective mass diffusivity are usually obtained from regression of a nonlinear model to the experimental data (Wang and Sun, 2003).

Accordingly, this work aimed at developing FEM numerical models to predict moisture content and size of gels slices of cornstarch and calcium alginate during convective drying. Values of effective mass diffusivity were obtained from nonlinear fitting of simulated drying profiles against experimental counterparts. Volumetric shrinkage of gel slices was experimentally measured and then compared to drying models. FEM simulation was accomplished via COMSOL Multiphysics v5.2 by coupling mass and momentum transport to shrinkage effects while geometry deformation was simulated by ALE method.

2. Material and methods

2.1. Material

Native cornstarch (Ingredion Ingredientes Industriais SA, Brazil), with moisture of 12.8% ± 2%, and sodium alginate (Protanal VK14, FMC Biopolymer, Brazil) were used to formulate the aqueous suspensions of cornstarch-alginate. Absolute ethanol (Dynamics, Brazil) was used as surfactant and increased the dispersion of sodium alginate powder in distilled water. Calcium chloride dihydrate (Sigma-Aldrich, Brazil) was used to prepare 1% w/v aqueous solutions.

2.2. Preparation of cornstarch-alginate suspensions and ionic gelation

Table 1 lists the formulation of cornstarch-alginate suspensions containing fractions of 50% (RC50 and GC50) and 90% (RC90 and GC90) of cornstarch, on dry basis. Fractions of sodium alginate, distilled water and ethanol used in the preparation of the suspensions are also reported. Sodium alginate powder was previously dispersed in ethanol and acted as surfactant towards better dispersion of alginate on water.

Cornstarch-alginate suspensions were placed within 27.8 mm PVC cylindrical tubes and immersed into 1% aqueous calcium chloride solution for 24 h. After the ionic gelation step, samples were cut into 5 mm thick slices. Gels were classified into 4 groups (namely RC50, RC90, GC50 and GC90) according to starch concentration and heat treatment. Samples RC50 and RC90 referred to formulations with 50% and 90% of native cornstarch, respectively, and they were not subjected to heat treatment. Samples GC50 and GC90 respectively referred to formulations with 50% and 90% of gelatinized cornstarch and they were immersed into distilled water at 80 °C for 1 h. Heat treatment aimed at promoting the gelatinization of native cornstarch, thus modifying the solid matrix.

Table 1
Formulation of cornstarch-alginate suspensions and cornstarch fractions on dry basis.

Sample	RC50	RC90	GC50	GC90
Cornstarch (g/100 g d.b.)	50	90	50	90
Cornstarch (g/100 g w.b.)	5.4	34.0	5.4	34.0
Water (g/100 g w.b.)	86.1	60.1	86.1	60.1
Sodium alginate (g/100 g w.b.)	4.7	3.3	4.7	3.3
Ethanol (g/100 g w.b.)	3.7	2.6	3.7	2.6
[a]Temperature of gelatinization step (°C)	n.a.	n.a.	80	80

[a] Thermal treatment considering the temperature of 80 °C, in a period of 60 min.

2.3. Convective drying experiments

Convective drying of gels slabs was performed in a drying tunnel with 10 cm × 10 cm square cross-section and 1 m length. Samples were placed at the tunnel dryer center and their weight was measured each 60-s intervals by a precision balance coupled to data acquisition system via communication port interface and MATLAB R2015a software. Drying air was heated by 2100 W electrical resistance coupled to PID temperature controller (NOVUS N1100, Brazil). Drying air temperature was set at (50, 60 and 70) °C while mean air velocity was kept at 0.5 m/s.

Gels slices with 24.8 mm ± 1.9 mm diameter and 4.9 mm ± 0.6 mm thickness were submitted to convective drying at temperatures of (50, 60 and 70) °C. Corresponding drying kinetics profiles were obtained for all formulations in Table 1 (RC90, GC90, RC50 and GC50) on dry basis with drying time ranging from 120 to 480 min, according to drying conditions and up to moisture equilibrium. An extra drying step at 105 ± 5 °C and under 24 h computed the dry weight and equilibrium concentration of samples (AOAC, 2005).

Experimental trials and drying profiles were carried out in triplicates for RC50, RC90, GC50 and GC90 formulations as well as drying temperatures of (50, 60 and 70)°C. Origin 2016 software averaged the experimental curves so that 12 experimental drying kinetics profiles were obtained.

From known values m_T of mass sample and m_d of mass of solids in samples on dry basis, moisture content X on dry basis was then evaluated as:

$$X = \frac{m_T - m_d}{m_d} \quad (1)$$

Where as moisture ratio XR was determined according to:

$$XR = \frac{X_t - X^{eq}}{X^0 - X^{eq}} \quad (2)$$

in which X^{eq} is the equilibrium moisture on dry basis, X^0 is the initial moisture on dry basis and X_t is the moisture on dry basis at time t.

2.4. Experimental measurements of volume shrinkage

Shrinkage was determined by additional drying experiments carried out at 60 °C. A micrometer was used to manually measure diameter and thickness of samples in order to compute their volumes every 10 min. Weight of samples was determined by a precision balance and moisture content on dry basis (X) was then obtained. Shrinkage was calculated as the ratio V/V^0, where V is the dry sample volume and V^0 is the wet sample initial volume.

2.5. Differential scanning calorimetry (DSC)

Differential scanning calorimetry (DSC) was analyzed using TA2010 equipment controlled by TA 4000 module (TA Instruments, USA) and accessory for cooling (Sobral et al., 2001). DSC capsules were prepared by initially depositing 6 mg of samples in DSC aluminum capsule together with distilled water to achieve a suspension of approximately 80% water in wet basis. Hydration time of samples was 2 h and samples were then heated from 20 °C to 120 °C at 10 °C/min rate. DSC thermograms showed the cornstarch gelatinization profile for samples that were not submitted to 80 °C thermal treatments, resulting in the

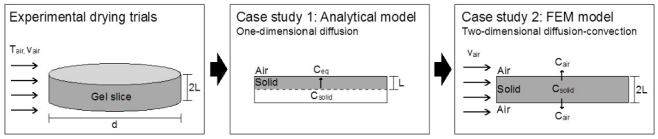

Fig. 1. Convective drying models put forward in case studies 1 and 2.

measurement of T_o (initial temperature), T_p (peak temperature), T_c (temperature of completion) and ΔH (gelatinization enthalpy) (Han and BeMiller, 2007; Pereira et al., 2010).

2.6. Scanning electron microscopy (SEM)

Microstructure of dried cornstarch-alginate samples was characterized through scanning electron microscopy (SEM) analyzes with Hitachi TM3000 electronic microscope (Hitachi, Japan). SEM images were able to show solid matrix morphology as well as homogeneity on surface and inside of dried gels. Electron source for SEM was a tungsten filament with 15 kV voltage and images were obtained in magnifications ranging from ×50 to ×1500.

3. Mathematical modeling of drying kinetics

With respect to the mathematical modeling of drying kinetics, this work considered two case studies as sketched in Fig. 1 and shortly addressed ahead. Shrinkage due to moisture loss refers to volume decrease during dehydration of samples. While analytical solutions are usually deduced under a number of simplifications, model sophistication may not guarantee quality inasmuch as complexity can go only to the point where key parameters can be compared with experimental data (de Souza-Santos, 2010). Accordingly, analytical solutions are stepping stones towards more complicated systems. In this work, analytical solutions denoted the exact solutions for simplified system, while numerical methods were applied to more complicated physical geometries and which are not possible to solve analytically.

Cornstarch-alginate gels were sliced into circular-flat slabs (i.e. discs). In view of that, either one-dimensional or two-dimensional mass transfer models can be proposed and tested so as to obtain drying profiles of flat slabs. Those drying models assumed negligible heat transfer as well as constant properties of drying air and constant volumetric concentration of dry solids (Curcio and Aversa, 2014; Ruiz-López et al., 2012).

Table 2 summarizes mathematical models and assumptions considered in case studies 1 and 2. Case study 1 refers to the analytical model based on Fick's Second Law for slab geometry and hence it relies solely on diffusive mass transfer. Case study 2 couples partial differential equations concerning mass transfer, fluid flow and geometry shrinkage (ALE method) and it was numerically solved by finite elements method (FEM) via COMSOL Multiphysics software.

3.1. Case study 1: analytical solution of Fick's second law

By considering constant effective diffusion coefficient D_{eff}, one-dimensional transient diffusion in Cartesian coordinates becomes:

$$\frac{\partial c}{\partial t} - D_{eff}\left(\frac{\partial^2 c}{\partial z^2}\right)=0 \tag{3}$$

in which $c = c(z,t)$ is water concentration (mol·m^{-3}) at any position z (m) in slab and time t (s). Uniform moisture X^0 was initially assumed throughout gel slab (including its surface), i.e. $X(z,0) = X^0$. Water concentration on slab surface was kept constant, $X(L,t) = X^{eq}$ (i.e. non-null Dirichlet boundary condition) where as symmetry is assumed about slab centerline, $\partial X/\partial z = 0$ at $z = 0$ (i.e. null Neumann condition).

In this case study, gel slab thickness was assumed to remain constant at its initial value $2L$ (m) so that $L = L_0$ is the corresponding half-thickness. Accordingly, the total amount XR of moisture that migrated from gel sample to drying air was determined by the analytical solution of Fick's second law in Cartesian coordinates (Crank, 1975):

$$XR = \sum_{n=0}^{\infty} \frac{8}{(2n+1)^2\pi^2} Exp\left(-\frac{(2n+1)^2\pi^2 D_{eff}\, t}{4L^2}\right) \tag{4}$$

3.2. Case study 2: finite-elements computational modeling

Case study 2 was implemented via finite element method (FEM) in COMSOL Multiphysics 5.2 by coupling fluid (i.e. drying air) flow to mass (i.e. moisture) transfer. The FEM model simulated the convective drying described by partial differential equations and with simultaneous evaluation of shrinkage. Specifically, Fick's second law was combined with convective moisture transfer in drying air as:

$$\frac{\partial c_1}{\partial t} - D_{air}\nabla^2 c_1 + v\cdot\nabla c_1=0 \tag{5}$$

in which D_{air} is effective water diffusivity in drying air and v is air flow velocity. Mass conservation within air velocity domain was implemented as:

$$\rho_1(\nabla\cdot v)=0 \tag{6}$$

By considering two-dimensional transient model and incompressible flow, drying air velocity (v) flowing around gel slabs was computed from Navier-Stokes equations:

$$\rho_1\frac{\partial v}{\partial t} + \rho_1(v\cdot\nabla)v = \nabla\cdot[-P + \mu(\nabla v + (\nabla v)')] + F \tag{7}$$

in which P referred to pressure term and F is external forces (e.g. gravity).

As far as gel slabs domain is concerned, only diffusive mass transfer was considered:

$$\frac{\partial c_2}{\partial t} - D_{eff}\nabla^2 c_2=0 \tag{8}$$

Table 2
Summary of mathematical models for convective drying in case studies 1 and 2.

Case study	Case 1	Case 2
Mass transfer	One-dimensional transient diffusion	Two-dimensional transient diffusion and convection
Mathematical model	Analytical model of Fick's Second Law	FEM numerical model with coupling of Fick's Second Law, external convection and geometry shrinkage
Moving boundary shrinkage model	$L = L_0$	$\frac{\partial L}{\partial t} = \frac{J_n M_w}{\rho_w}$
Initial moisture within solid domain	$c_2(z, 0) = c_2^0$	$c_2(z, 0) = c_2^0$
Boundary concentration constraint $t > 0$	$c_2(L, t) = c_2^{eq}$	$K_p = \frac{c_1^{sat}}{c_2^{eq}}$
Concentration axis symmetry	$\frac{\partial c_2}{\partial z} = 0$, at $z = 0$	n.a.
Water concentration in inlet air	n.a.	$c_1(t) = c_1^0$
Inlet air velocity	n.a.	$v = v_1$

FEM model considered the solid matrix as being isotropic during computation of diffusivity mass transfer coefficients.

3.2.1. Description of molar concentration within hot air

Ideal gas law was invoked to assess the molar concentration of water c_1^0 (mol·m^{-3}) in drying air at dryer inlet. Accordingly, if P_w (Pa) is partial pressure of water and T (K) is drying air temperature, the following expression holds:

$$c_1^0 = \frac{P_w}{RT} \tag{9}$$

being $R = 8.314$ J·mol^{-1}·K^{-1} the ideal gas constant. Partial pressure of water was obtained from relative humidity of air room (RH_T) together with saturation pressure (P_T^{sat}) as:

$$P_w = RH_T P_T^{sat} \tag{10}$$

This relation is valid for isobaric heating of room air to the drying temperature. Saturation pressure P_T^{sat} (Pa) was determined from Tetens equation for temperatures T (K) above water freezing point (Murray, 1967), namely:

$$P_T^{sat} = 610.78\, Exp\left(\frac{17.2693882\ (T - 273.16)}{(T - 35.96)}\right) \tag{11}$$

3.2.2. Molar concentration in wet samples

If W (kg/kg-wb) is moisture content in wet basis and m_T (kg) is the total mass of wet solid (gel slab), the number of moles of water (N_w) was obtained from its mass ($m_w = m_T{\cdot}W$) and molecular weight ($M_w = 18.01528$ g·mol^{-1}) as:

$$N_w = \frac{m_T\, W}{M_w} \tag{12}$$

The initial molar concentration of water c_2^0 (mol·m^{-3}) in wet solid was obtained from the number of moles (N_w) and the total volume (V^0) of gel slab as:

$$c_2^0 = \frac{N_w}{V^0} \tag{13}$$

Let $\rho_2 = m_T/V^0$ be solid density (kg·m^{-3}). By inserting Eq. (12) into Eq. (13) while converting wet-basis moisture W into dry-basis counterpart X (kg·kg-d.b.$^{-1}$), one then obtains:

$$c_2^0 = \frac{\rho_2}{M_w}\frac{X^0}{(1 + X^0)} \tag{14}$$

which relates water concentration c_2 to moisture content X.

3.2.3. Equilibrium concentration and partition coefficient

Case 2 assumed water concentration at air-solid boundary is related to the equilibrium condition and it is obtained from water saturation pressure as follows:

$$c_1^{sat} = \frac{P_T^{sat}}{R\ T} \tag{15}$$

Partition coefficients K_p were then determined from water vapor concentration in air (c_1^{sat}) and equilibrium concentration on sample surface (c_2^{eq}) over the drying time as follows:

$$K_p = \frac{c_1^{sat}}{c_2^{eq}} \tag{16}$$

3.2.4. Shrinkage modeling by computing total normal flux (case 2)

Total normal molar flux J_n (mol·m^{-2}·s^{-1}) was computed over geometry boundaries as:

$$J_n = -D_{eff}\nabla c \tag{17}$$

Case study 2 assumed that shrinkage was obtained from volume reduction on wet solid due to moisture loss through drying surfaces. Based on the normal molar flux, moving boundary velocity $\overrightarrow{v_n}$ (m·s^{-1}) was then determined as:

$$\overrightarrow{v_n} = -\frac{\partial L}{\partial t} = -\frac{J_n\, M_w}{\rho_w} \tag{18}$$

The FEM model evaluated the water molar flux on solid boundaries, which was used to compute the moving boundary velocity, simultaneously. In sequence, the moving boundary velocity was used in ALE method to account shrinkage. The built-in moving mesh toolbox was used to numerically simulate shrinkage by the Arbitrary Lagrangian-Eulerian (ALE) method (Ajani et al., 2017; Sun et al., 2011).

3.3. Solver of mathematical models

By considering the boundary conditions listed in Table 2, those models were fitted to experimental data. Specifically, effective mass diffusivity D_{eff} (m^2·s^{-1}) was obtained by nonlinear fitting of diffusion models against experimental drying kinetics, i.e. D_{eff} resulted from the smallest deviation between experimental and simulated data. While Mathematica Wolfram v.11.2 software performed least-squares regression through Levenberg-Marquadt method, COMSOL Multiphisics v5.2 software used BOBYQA optimization method.

Coefficient of determination (R^2) and mean square error (RMSE) were used as goodness of fit parameter, namely:

$$R^2 = 1 - \left(\frac{\sum_i^N (O_i - P_i)^2}{\sum_i^N (O_i - \overline{P_i})^2}\right) \tag{19}$$

$$RMSE = \left(\sum_i^N \frac{(O_i - P_i)^2}{N}\right)^{\frac{1}{2}} \tag{20}$$

in which P_i and O_i refer to experimentally observed and numerically simulated values, respectively, and N is the number of observations in the data set. Best-fit was assumed when RMSE was minimized and R^2 was maximized.

4. Results and discussion

4.1. Solid domain: characterization of the cornstarch-alginate gel slabs and dried solids

Table 3 shows diameters and thicknesses of gel slab samples. Slab diameter ranged from 22 mm to 27 mm while thickness ranged from

Table 3
Characterization of cornstarch-alginate gels and dried solid.

Parameter	RC50	RC90	GC50	GC90
d, Diameter of gel slab (mm)	24.8 ± 0.3	25.0 ± 0.4	22.3 ± 0.3	27.0 ± 0.3
δ, Thickness of gel slab (mm)	4.6 ± 0.6	4.6 ± 0.5	4.1 ± 0.2	4.9 ± 0.4
ρ_2, Solid density of gel slab (kg·m^{-3})	1055.3^a ± 3.6	1186.7^b ± 46.4	1061.2^a ± 9.3	1160.7^b ± 23.9
ρ_2^d, Solid density of dried slab (kg·m^{-3})	1849.4^a ± 94.9	1657.5^b ± 24.7	1928.6^a ± 91.7	1826.9^a ± 81.1
V/V^o, Total shrinkage (−)	11.6% ± 1.4%	53.8% ± 3.5%	15.3% ± 1.7%	54.2% ± 3.6%

Samples that are not significantly different one each other are represented with the same letter, at the 95% confidence level.

4.1 mm to 4.9 mm. The size of GC50 and GC90 samples changed during heat treatment at 80 °C, which led to cornstarch gelatinization as well.

Solid densities of gel slabs were measured via water pycnometry, being above 1160 $kg{\cdot}m^{-3}$ for formulations with 90% cornstarch (i.e. RC90 and GC90). Gels with 50% cornstarch presented solid densities below 1061 $kg{\cdot}m^{-3}$. Statistics analysis from Tukey test compared mean values of densities. The density of moist gel slabs can be statistically grouped according to their cornstarch fractions: 50% or 90%. Samples RC50 and GC50 showed similar densities with no significant difference while samples RC90 and GC90 constituted another group. In contrast, the densities of dried gel slabs showed no significant difference between samples RC50, GC50 and GC90, with values ranging from 1826.9 to 1928.6 $kg{\cdot}m^{-3}$. The density of dried sample RC90 is relatively lower probably due to the presence of internal pores.

Solid densities of dried solids were measured via helium gas pycnometry. As Table 3 shows, samples with higher starch fractions (RC90 and GC90) presented lower solid densities than samples with higher concentration of calcium alginate (GC50 and RC50).

Solid densities of either wet or dried gel slabs are related to their composition and they could be estimated from a weighted average of densities of each ingredient (Choi et al., 1986). Dried cornstarch has solid density around 1862 $kg{\cdot}m^{-3}$ while solid density of pure calcium alginate beads is 2386.8 $kg{\cdot}m^{-3}$ (Feltre et al., 2018).

Samples with higher starch concentration (RC90 and GC90) presented lower water fraction and the final volume was around 54% in relation to the initial volume. Samples with higher water fraction (RC50 and GC50) presented more size reduction so that the final volume was between 11.6% and 15.3% in relation of the initial volume, respectively.

Fig. 2 shows microstructure details of dried cornstarch-alginate gels. SEM images were obtained for RC50, RC90, GC50 and GC90 samples dried at 50, 60 and 70 °C.

SEM images of RC50 and RC90 samples show native cornstarch granules with preserved microstructure for any drying temperature. With 50% alginate and 50% cornstarch, RC50 samples (Fig. 2a–c) showed native cornstarch fully immersed in calcium alginate matrix. Increasing drying temperature from 50 °C to 70 °C resulted in internal cracking of solid matrix. Such cracking phenomenon was probably due to higher drying rate leading to faster water loss. RC50 solids showed more compact microstructure with higher solid densities than those of RC90 samples.

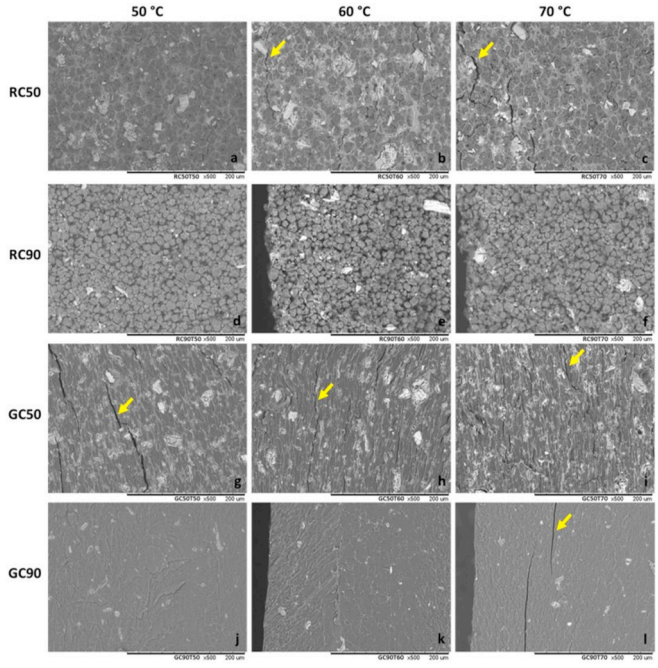

Fig. 2. Internal microstructure of dried cornstarch-alginate solids observed from SEM images at ×500 magnification, with arrow markers indicating the internal cracking.

RC90 samples (Fig. 2d–f) showed some internal pores and native cornstarch granules were agglomerated by calcium alginate solid bridges. Solid density of RC90 samples (1657.5 $kg{\cdot}m^{-3}$) was lower than native cornstarch density (1862 $kg{\cdot}m^{-3}$), thus evidencing the presence of occluded internal pores in its solid matrix.

SEM images of GC50 and GC90 samples showed the deformation on native cornstarch microstructure. In contrast to samples containing raw cornstarch (RC50 and RC90), it is not possible to observe well-defined and rounded cornstarch granules on SEM images of gelatinized samples (GC50 and GC90). These samples were previously submitted to heat treatment at 80 °C so that native cornstarch was completely gelatinized.

GC50 samples (Fig. 2g–i) also showed internal cracking for all drying temperatures. Higher amount of calcium alginate combined with starch gelatinization resulted in higher compaction of GC50 samples, which presented the highest solid density (1928.6 $kg{\cdot}m^{-3}$).

GC90 samples (Fig. 2j–l) have homogeneous microstructure, as observed by cornstarch dispersion in alginate gel. Internal cracking was only observed at 70 °C (GC90T70) for higher drying.

Differential scanning calorimetry analysis (DSC) computed gelatinization peak temperatures of samples with native cornstarch RC50 and RC90, as described in Table 4. RC50 samples had higher alginate concentration and compaction than RC90 samples and gelatinization temperature peak shifted from 71 °C to 83 °C, respectively. Gelatinization enthalpy values indicate that the energy required to gelatinize cornstarch was similar in all formulations. GC50 and GC90 samples contained gelatinized cornstarch and they did not show any peak in DSC analyzes.

4.2. Operating parameters related to drying temperature

Drying experiments used air at 50, 60 and 70 °C and Table 5 shows some air and water thermophysical properties at aforesaid temperatures. Relative air humidity values were experimentally determined at room temperature. Some air and water vapor properties were extracted from the literature (Bergman et al., 2011). Diffusion coefficients of water vapor in air (D_{air}) were estimated via Chapman-Enskog theory and Lennard-Jones potential parameters (Cussler, 2009). All parameters and properties here in listed were used in drying models in order to simulate drying profiles.

4.3. Fixed operational parameters

Table 6 shows parameters that remained fixed in drying experiments and, therefore, numerical simulations. Both temperature and relative humidity of room air were monitored, and air velocity was kept at 0.5 $m{\cdot}s^{-1}$ in all drying experiments.

4.4. Water molar concentration and partition coefficient

Table 7 shows moisture content results for cornstarch-alginate samples. Initial moisture on dry basis (X^0) and equilibrium moisture (X^{eq}) were used to compute initial molar concentration (c_2^0) and equilibrium concentration (c_2^{eq}), according to Eq. (14). Table 7 also shows water vapor concentration values at air-solid boundary (c_1^{sat}), as determined from water saturation pressure according to Eq. (11), and partition coefficient (K_p) as computed from Eq. (16).

RC50 and GC50 samples presented higher water concentration than RC90 and GC90 samples, which contained higher starch fractions. Moisture decreased proportionally with drying and samples with higher initial water content also presented higher equilibrium concentrations. Heat treatment led to native cornstarch gelatinization as well as decrease of equilibrium concentration of gelatinized samples, when

Table 4
Thermal analysis data and standard deviation (To, Tp, Tc, ΔH and ΔHadj) for dried cornstarch-alginate samples.

Sample*	To (°C)	Tp (°C)	Tc (°C)	ΔH (J/g)	ΔHadj** (J/g)
RC50T50	70.58 ± 1.76	83.32 ± 2.08	98.66 ± 2.47	1.05 ± 0.47	7.51 ± 0.86
RC50T60	68.42 ± 1.92	80.54 ± 2.26	95.18 ± 2.68	1.32 ± 0.11	10.28 ± 0.62
RC50T70	70.23 ± 1.47	83.94 ± 1.76	98.36 ± 2.07	1.28 ± 0.23	6.59 ± 1.36
RC90T50	66.16 ± 1.19	71.51 ± 1.29	78.66 ± 1.42	1.37 ± 0.19	6.61 ± 1.13
RC90T60	64.88 ± 0.97	72.1 ± 1.08	83.44 ± 1.25	2.11 ± 0.17	9.00 ± 0.98
RC90T70	65.26 ± 1.11	70.81 ± 1.02	81.27 ± 1.38	2.12 ± 0.15	10.27 ± 0.85

*GC50 and GC90 samples showed no gelatinization peaks.
** To is the initial temperature, Tp is the peak temperature, Tc is the temperature of completion of DSC event and ΔH is the gelatinization enthalpy.
***ΔHadj corresponds to gelatinization enthalpy adjusted in mass basis of per gram of cornstarch.

Table 5
Air and water properties related to drying temperatures considered in this work.

Parameter	Drying conditions		
T, Drying temperature (°C)	50	60	70
ρ_1, Air density (kg/m^3)	1.091	1.058	1.028
RH, Relative humidity of inlet hot air (−)	14.7%	11.8%	5.4%
D_{air}, Diffusivity of water on air (cm^2.s^{-1})	0.292	0.309	0.327
ρ_w, Water liquid density (kg·m^{-3})	988.04	983.20	977.77
P^{sat}, Saturation pressure of water vapor (Pa)	12348	19953	31251

Table 6
Fixed parameters of convective drying.

Parameter	Value
v_1, Inlet air velocity (m.s^{-1})	0.5 ± 0.05
T_{room}, Room air temperature (°C)	27 ± 2
RH_{room}, Room air relative humidity (−)	51% ± 6%
Y, Height of dryer tunnel (m)	0.10
Z, Length of dryer tunnel (m)	1.0
M_w, Water molar mass (kg·mol^{-1})	0.018015
Rs, Ideal gas constant (J·mol^{-1}K^{-1})	8.3145

compared to non-gelatinized ones (e.g. GC50 samples showed lower equilibrium concentrations than RC50 samples). Similar behavior was observed between GC90 and RC90 samples and it might be explained in terms of native cornstarch microstructure.

Native non-gelatinized cornstarch granules absorbed water by amylopectin and amylose helical structures, resulting in granules swelling (Sajilata et al., 2006). Native cornstarch showed better organized structure than gelatinized cornstarch and it retained more water during convective drying. In view of that, equilibrium concentration of non-gelatinized samples was higher. On the other hand, the helical structure of cornstarch was disrupted with gelatinization, thus resulting in greater dehydration of samples subjected to heat treatment.

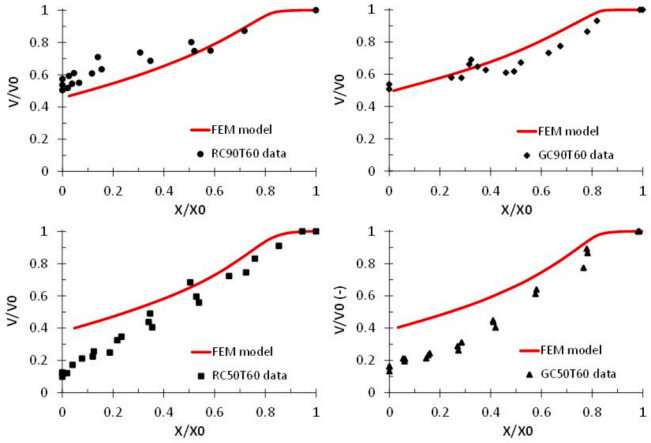

Fig. 3. Experimental data and simulated results of volumetric shrinkage of slabs in relation to dimensionless moisture on dry basis.

4.5. Description of volume shrinkage with moisture content

Fig. 3 shows experimental shrinkage data and respective FEM model results related to samples dried under 60 °C. FEM model computed the free deformation over entire geometry boundaries. RC90 and GC90 gels samples, containing higher cornstarch fractions, showed a lower final shrinkage (53.8% and 54.2%) and FEM model simulated adequately the geometry deformation in relation to moisture removal of these samples. RC50 and GC50 gels samples has higher initial moisture content and showed a higher final shrinkage (11.6% and 15.3%). For these samples, FEM model did not predict adequately the shrinkage data when X/X^0 were lower than 0.6. The deviations between simulated and experimental results may be occurred by the solid microstructure heterogeneity, as well as dependency between modulus of elasticity and moisture content (Ajani et al., 2017).

Table 7
Drying temperature, moisture content and partition coefficients.

Sample	T(°C)	X^0(kg/kg)	X^{eq}(kg/kg)	c_2^0 (mol/m^3)	c_2^{eq} (mol/m^3)	c_1^{sat} (mol/m^3)	$K_p \times 10^4$(−)
RC50T50	50	9.21 ± 1.30	1.13 ± 0.10	52839.6	31059.4	4.6	1.48
RC50T60	60	12.58 ± 0.11	0.93 ± 0.05	54264.5	28195.2	7.2	2.55
RC50T70	70	8.62 ± 0.88	0.98 ± 0.21	52490.8	28918.3	11.0	3.79
RC90T50	50	1.87 ± 0.14	0.19 ± 0.03	42954.6	10733.6	4.6	4.28
RC90T60	60	1.89 ± 0.22	0.22 ± 0.04	43067.0	12077.0	7.2	5.96
RC90T70	70	1.71 ± 0.16	0.19 ± 0.03	41573.9	10283.8	11.0	10.7
GC50T50	50	7.36 ± 0.06	0.61 ± 0.01	51857.7	22284.1	4.6	2.06
GC50T60	60	7.51 ± 1.59	0.48 ± 0.08	51983.4	19068.6	7.2	3.78
GC50T70	70	6.63 ± 1.56	0.27 ± 0.04	51184.3	12577.9	11.0	8.71
GC90T50	50	2.30 ± 0.07	0.16 ± 0.04	44884.1	8886.7	4.6	5.17
GC90T60	60	2.52 ± 0.39	0.17 ± 0.01	46099.0	9525.7	7.2	7.56
GC90T70	70	2.42 ± 0.11	0.13 ± 0.01	45611.9	7235.0	11.0	15.10

Table 8
Effective mass diffusion coefficients obtained via cases study 1 and 2.

Sample	Case 1: Analytical model			Case 2: FEM model		
	$D_{eff} \times 10^4$ (m^2/s)	RMSE	R^2	$D_{eff} \times 10^4$ (m^2/s)	RMSE	R^2
RC50T50	5.77	0.0618	0.9702	4.20	0.0269	0.9908
RC50T60	8.06	0.0771	0.9581	5.46	0.0343	0.9865
RC50T70	11.63	0.0717	0.9578	6.58	0.0581	0.9585
RC90T50	6.71	0.0558	0.9631	3.64	0.0560	0.9510
RC90T60	8.66	0.0515	0.9654	4.42	0.0632	0.9337
RC90T70	12.13	0.0610	0.9635	6.16	0.0703	0.9321
GC50T50	4.98	0.0520	0.9736	3.39	0.0235	0.9921
GC50T60	6.26	0.0516	0.9741	3.78	0.0301	0.9869
GC50T70	7.74	0.0551	0.9705	4.40	0.0346	0.9831
GC90T50	3.29	0.0168	0.9972	1.65	0.0768	0.8967
GC90T60	4.74	0.0144	0.9975	2.38	0.0575	0.9381
GC90T70	5.22	0.0104	0.9984	2.77	0.0503	0.9439

4.6. Mathematical modeling of convective drying

Table 8 presents effective mass diffusivities (D_{eff}) obtained by least-square regression from drying models proposed in case studies 1 and 2. All models were fitted to experimental data and goodness-of-fit tests RMSE and R^2 indicated low discrepancy between observed and predicted values. The fitting coefficients indicated that the analytical model (Case 1) fitted better the experimental data of RC90 and GC90 samples, while FEM model (Case 2) fitted better results of RC50 and GC50 samples.

Case 1 model considered the analytical solution of Fick's second law with no shrinkage effects, being adequate to describe the drying kinetics of materials with lower shrinkage ratios and lower initial moisture content, such as RC90 and GC90 samples.

In special, drying of GC90 samples showed the slowest drying rate so that moisture reached equilibrium after 21600 s (6 h), as observed in Fig. 4(d1-d2). Cornstarch gelatinization produced a more homogeneous cornstarch-alginate matrix where water was uniformly absorbed by the solid, resulting in a lower shrinkage when compared to gel samples containing raw cornstarch. As the result, diffusion coefficients obtained for GC90 samples ranged from $3.29 \times 10^{-10}\,m^2{\cdot}s^{-1}$ (GC90T50) to $5.22 \times 10^{-10}\,m^2{\cdot}s^{-1}$ (GC90T70), being the lowest ones when compared to others groups.

Case 1 model also had a good fit for RC90 samples, which contained 90% native cornstarch. RC90 samples have heterogeneous solid matrix, where in native cornstarch granules were agglomerated by calcium alginate bindings, as shown by SEM images on Fig. 2. As described in Fig. 4 (b1-b2), equilibrium moisture of RC90 samples was reached at 10800 s (3 h), being half of drying time obtained for GC90 samples. Diffusion coefficients obtained for RC90 group ranged from $6.71 \times 10^{-10}\,m^2{\cdot}s^{-1}$ (RC90T50) to $12.13 \times 10^{-10}\,m^2{\cdot}s^{-1}$ (RC90T70), being higher than GC90 samples.

The constant-rate period of drying profile has been traditionally linked to evaporation of free water on solid surface. However, a similar constant-rate period is observed on solids containing water uniformly bound on solid matrix when shrinkage is observed (Valentas et al., 1997). In this case, shrinkage reduces surface area of solids and drying rate shows a constant period with moisture content decrease, which is referred to as pseudo-constant rate.

Samples containing 50% cornstarch (RC50 and GC50) had initial moisture content around 86.1 g/100 g wb and a higher shrinkage was observed. Case 1 model did not explain the pseudo-constant drying rate period and Case 2 had a better fitting for both RC50 and GC50 samples. COMSOL FEM model included shrinkage effects and better explained the pseudo-constant drying rate from 0 to 3000 s, when linear decrease

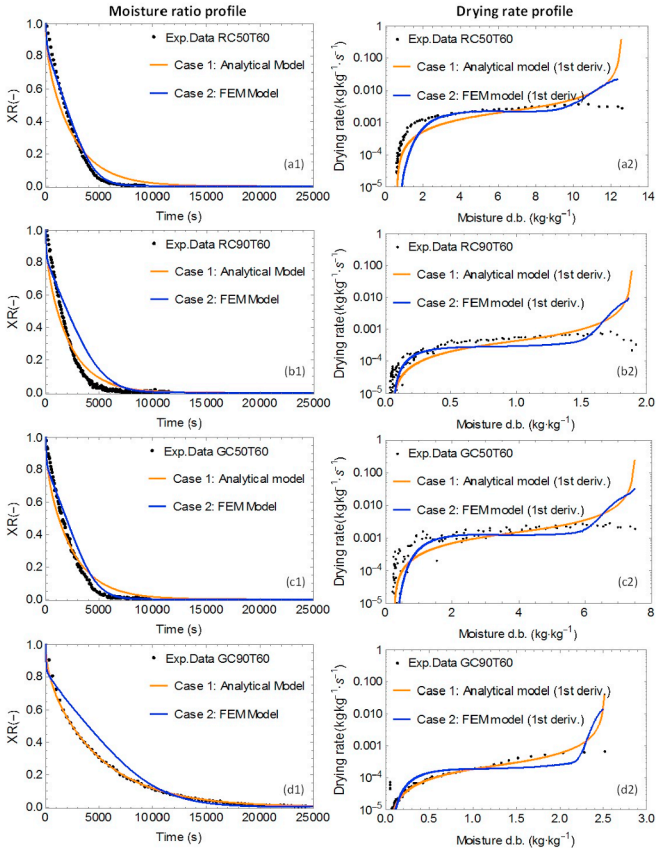

Fig. 4. Experimental drying profiles and best-fitting numerical counterparts as obtained from models proposed in case studies 1 and 2.

of moisture ratio (XR) is observed, as shown in Fig. 4(a1-a2) and Fig. 4(c1-c2). This phenomenon corroborated with previous studies on drying of foods by considering shrinkage effects (Valentas et al., 1997).

Samples containing 50% of non-gelatinized starch (RC50) presented diffusion coefficients in the range from $4.20 \times 10^{-10}\,m^2{\cdot}s^{-1}$ (RC50T50) to $6.58 \times 10^{-10}\,m^2{\cdot}s^{-1}$ (RC50T70). These values were higher than diffusion coefficients obtained for samples containing 50% gelatinized starch (GC50), which varied from $3.39 \times 10^{-10}\,m^2{\cdot}s^{-1}$ (GC50T50) to $4.40 \times 10^{-10}\,m^2{\cdot}s^{-1}$ (GC50T70).

Cornstarch gelatinization resulted in greater capacity of solid matrix to bind water. In view of that, the drying rate of gelatinized gels became lower when compared with samples containing native cornstarch. As a result, effective diffusion coefficients were lower in solids containing gelatinized starch (Lv et al., 2011).

The magnitude order of diffusion coefficients obtained in this work are in agreement to effective diffusivities of food materials, which range from 10^{-11} to $10^{-9}\,m^2{\cdot}s^{-1}$ (Khan et al., 2017). Because of cornstarch-alginate gel slabs are composed by foodstuffs, their drying profiles were similar to drying profiles of food materials.

Fig. 4 (a2, b2, c2 and d2) illustrates the drying rate profiles obtained from first order derivative of drying models. Case study 1 model better described the drying of RC90 and GC90 samples, showing a falling rate period over all drying time, thus evidencing traditional Fickian diffusion behavior. COMSOL FEM model (Case 2) presented good fit for both RC50 and GC50 samples with higher shrinkage, and well described the pseudo-constant period on drying rate profiles.

Constant-rate periods presented on drying profiles are commonly associated to removal of unbound water on food products (Heldman and Lund, 2006). However, this work evidenced the presence of a

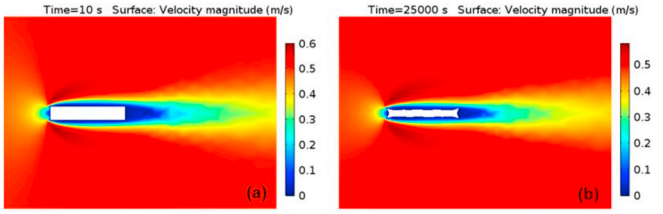

Fig. 5. Air velocities profiles obtained in case study 2 (FEM model) describing air flow patterns over gel slabs during convective drying.

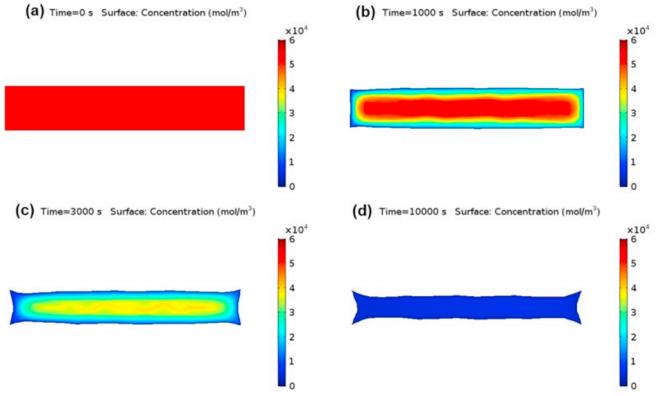

Fig. 6. Water molar concentration profiles obtained in case study 2 (FEM model) for RC50T50 samples.

pseudo-constant drying rate on materials showing higher shrinkage ratio, in which surface area varied during drying.

4.7. Two-dimensional profiles obtained from case study 2 modeling

FEM model (Case 2) computationally simulated the two-dimensional air flow profile of drying air over gel slabs, as shown in Fig. 5. Inlet air velocity was equal to 0.5 m/s and a velocity profile around the solid boundaries was computed, from which convective mass (i.e. moisture) transfer was estimated in air domain. Shrinkage led to sample flatness so that air velocity profile changed during drying. Fig. 5a and b illustrate velocity profiles at initial (10 s) and final (25000 s) instants, respectively.

FEM model also determined molar concentration profiles of water in solid domain. Fig. 6 shows moisture distribution within slab as well as its 2D shape was simulated at drying instants of 0, 1000, 3000 and 10000 s. Moisture profiles also show the volume reduction due to water migration from gel slabs, which resulted in their shrinkage. Cuneiform edges were numerically computed in dehydrated slabs and this phenomenon was also observed in experimental samples. The 90° solid edges were quickly dried so that the solid matrix become stiff in these portions, rendering higher thickness at those edges in relation to dried slab center.

Fig. 6b and c shows faster shrinkage with lower moisture on the left side (i.e. inlet air) due to higher convective mass (moisture) transfer and higher drying rate. However, after (completely) drying the solid, slab edges became roughly the same on both sides (i.e. upstream and downstream edges). The shape of experimental samples presented small curvatures on drying, which is prospectively due to the dependence between elastic modulus and moisture content (Ajani et al., 2017).

5. Conclusion

Fick's diffusion model described the drying of cornstarch-alginate gel slabs through both analytical and numerical (i.e. FEM) methods. Shrinkage was incorporated into models, thus better explaining drying profiles. Effective mass diffusivity was a transport parameter invoked in all case studies, whose best-fitted value ranged from 3.3×10^{-10} m^2·s^{-1} to 12.1×10^{-10} m^2·s^{-1}.

Samples containing higher amount of gelatinized or raw cornstarch (GC90 and RC90) were better fitted by the analytical solution of Fick's second law (Case study 1). Case 1 model did not considered shrinkage effects and a falling rate period over all drying time was observed.

In other hand, samples containing higher amount of water (RC50 and GC50) presented increased shrinkage ratios and were better fitted by COMSOL FEM model (Case study 2). In these cases, drying showed a pseudo-constant rate period, resulting in lower drying time towards equilibrium moisture.

Gelatinization of cornstarch produced lower shrinkage ratios, evidencing a stronger water binding in solid matrix with a slower drying, when compared to raw cornstarch samples.

Diffusive mass (moisture) transfer was the main mechanism in gels drying. However, shrinkage affected drying profiles of cornstarch-alginate gels, resulting in a pseudo-constant drying rate thus rendering higher drying rate. In addition, the inclusion of shrinkage effects is essential to better describe drying of biopolymers whose shape changes over drying.

Conflicts of interest

The authors declare no conflicts of interest.

Acknowledgements

This study was financed in part by the Coordenação de Aperfeiçoamento de Pessoal de Nível Superior - Brazil (CAPES) - Finance Code 001, and by the National Counsel of Technological and Scientific Development - Brazil (CNPq) - grant 445533/2014-5.

Nomenclature

c	Water concentration (mol·m^{-3})
D_{air}	Diffusivity of water in air domain (m^2·s^{-1})
D_{eff}	Effective diffusivity of water in solid domain (m^2·s^{-1})
H	Enthalpy (J·kg^{-1})
J_n	Total normal molar flux (mol·m^{-2}·s^{-1})
K_p	Partition coefficient (dimensionless)
k_i	Numerical constants of empirical equations (dimensionless)
L	Slab thickness (m)
M_w	Water molar mass (kg·mol^{-1})
m	Mass (kg)
N	Number of moles (mol)
P	Pressure (Pa)
R	Universal gas constant (J·mol^{-1}·K^{-1})
RH	Relative humidity (dimensionless)
$RMSE$	Root-mean-square error (dimensionless)
R^2	Coefficient of determination (dimensionless)
T	Air temperature (°C or K)
t	Time (s)
T_o	Initial temperature of DSC event (°C)
T_p	Peak temperature of DSC event (°C)
T_c	Temperature of completion of DSC event (°C)
V	Volume (m^3)
V/V^0	Shrinkage (dimensionless)
$\overrightarrow{v_n}$	Normal velocity of moving boundary (m·s^{-1})
X	Moisture content in dry basis (kg·kg^{-1})
XR	Moisture ratio (dimensionless)
ρ	Density (kg·m^{-3})
GC50	Dried samples containing 50% of gelatinized cornstarch
GC90	Dried samples containing 90% of gelatinized cornstarch
RC50	Dried samples containing 50% of native cornstarch
RC90	Dried samples containing 90% of native cornstarch

References

Ajani, C., Kumar, A., Curcio, S., Tekasakul, P., 2017. Parametric study and shrinkage modelling of natural rubber sheet drying using COMSOL multiphysics. IOP Conf. Ser. Mater. Sci. Eng. 243, 012012. https://doi.org/10.1088/1757-899X/243/1/012012.

AOAC, 2005. Official Methods of Analysis of AOAC International, eighteenth ed. Association of Official Analytical Chemists, Arlington, VA, USA.

Balanč, B., Kalušević, A., Drvenica, I., Coelho, M.T., Djordjević, V., Alves, V.D., Sousa, I., Moldão-Martins, M., Rakić, V., Nedović, V., Bugarski, B., 2016. Calcium-alginate-inulin microbeads as carriers for aqueous carqueja extract. J. Food Sci. 81, E65–E75. https://doi.org/10.1111/1750-3841.13167.

Bergman, T.L., Incropera, F.P., DeWitt, D.P., Lavine, A.S., 2011. Fundamentals of Heat and Mass Transfer. John Wiley & Sons.

Castro, A.M., Mayorga, E.Y., Moreno, F.L., 2018. Mathematical modelling of convective drying of fruits: a review. J. Food Eng. 223, 152–167. https://doi.org/10.1016/j.jfoodeng.2017.12.012.

Choi, Y., Okos, M.R., LEMAUGUER, M., JELEN, M., 1986. Food engineering and process applications: transport phenomena. Food Eng. Process Appl. Transp. Phenom. 1.

Crank, J., 1975. The Mathematics of Diffusion, second ed. Clarendon Press, Oxford.

Curcio, S., Aversa, M., 2014. Influence of shrinkage on convective drying of fresh vegetables: a theoretical model. J. Food Eng. 123, 36–49. https://doi.org/10.1016/j.jfoodeng.2013.09.014.

Cussler, E.L., 2009. Diffusion: Mass Transfer in Fluid Systems. Cambridge university press.

de Souza-Santos, M., 2010. Solid Fuels Combustion and Gasification: Modeling, Simulation, and Equipment Operations, second ed. Dekker Mechanical Engineering. CRC Press, Boca Raton, USA. https://doi.org/10.1201/9781420047509.

Defraeye, T., 2017. Impact of size and shape of fresh-cut fruit on the drying time and fruit quality. J. Food Eng. 210, 35–41. https://doi.org/10.1016/j.jfoodeng.2017.04.004.

Feltre, G., Silva, C.A., Lima, G.B., Menegalli, F.C., Dacanal, G.C., 2018. Production of thermal-resistant cornstarch-alginate beads by dripping agglomeration. Int. J. Food Eng. 14. https://doi.org/10.1515/ijfe-2017-0296.

Flores-andrade, E., Pascual-pineda, L.A., Jim, M., 2015. Effect of water activity on the stability of Lactobacillus paracasei capsules. LWT - Food Sci. Technol. 60, 346–351. https://doi.org/10.1016/j.lwt.2014.09.050.

Han, J.A., BeMiller, J.N., 2007. Preparation and physical characteristics of slowly digesting modified food starches. Carbohydr. Polym. 67, 366–374. https://doi.org/10.1016/j.carbpol.2006.06.011.

Heldman, D., Lund, D., 2006. Handbook of Food Engineering, second ed. Food Science and Technology. CRC Press. https://doi.org/10.1201/9781420014372.

Khan, M.I.H., Kumar, C., Joardder, M.U.H., Karim, M.A., 2017. Determination of appropriate effective diffusivity for different food materials. Dry. Technol. 35, 335–346. https://doi.org/10.1080/07373937.2016.1170700.

Kumar, C., Joardder, M.U.H., Farrell, T.W., Karim, M.A., 2016. Multiphase porous media model for intermittent microwave convective drying (IMCD) of food. Int. J. Therm. Sci. 104, 304–314. https://doi.org/10.1016/j.ijthermalsci.2016.01.018.

Kumar, C., Millar, G.J., Karim, M.A., 2015. Effective diffusivity and evaporative cooling in convective drying of food material. Dry. Technol. 33, 227–237. https://doi.org/10.1080/07373937.2014.947512.

Lv, X., Wu, L., Wang, J., Li, J., Qin, Y., 2011. Characterization of water binding and dehydration in gelatinized starch. J. Agric. Food Chem. 59, 256–262. https://doi.org/10.1021/jf103523u.

Mujumdar, A., 2006. Handbook of Industrial Drying, third ed. CRC Press. https://doi.org/10.1201/9781420017618.

Murray, F.W., 1967. On the computation of saturation vapor pressure. J. Appl. Meteorol. https://doi.org/10.1175/1520-0450(1967)006<0203:OTCOSV>2.0.CO;2.

Pereira, N.R., Godoi, F.C., Rocha, S.C.S., 2010. Drying of starch suspension in spouted bed with inert particles: physical and thermal analysis of product. Dry. Technol. 28, 1288–1296. https://doi.org/10.1080/07373937.2010.490891.

Perussello, C.A., Kumar, C., De Castilhos, F., Karim, M.A., 2014. Heat and mass transfer modeling of the osmo-convective drying of yacon roots (Smallanthus sonchifolius). Appl. Therm. Eng. 63, 23–32. https://doi.org/10.1016/j.applthermaleng.2013.10.020.

Raghavan, G.S.V., Tulasidas, T.N., Sablani, S.S., Ramaswamy, H.S., 1995. A method of determination of concentration dependent effective moisture diffusivity. Dry. Technol. 13, 1477–1488. https://doi.org/10.1080/07373939508917034.

Rojas-Moreno, S., Osorio-Revilla, G., Gallardo-Velázquez, T., Cárdenas-Bailón, F., Meza-Márquez, G., 2018. Effect of the cross-linking agent and drying method on encapsulation efficiency of orange essential oil by complex coacervation using whey protein isolate with different polysaccharides. J. Microencapsul. 35, 165–180. https://doi.org/10.1080/02652048.2018.1449910.

Ruiz-López, I.I., Ruiz-Espinosa, H., Arellanes-Lozada, P., Bárcenas-Pozos, M.E., García-Alvarado, M.A., 2012. Analytical model for variable moisture diffusivity estimation and drying simulation of shrinkable food products. J. Food Eng. 108, 427–435. https://doi.org/10.1016/j.jfoodeng.2011.08.025.

Sabarez, H.T., 2012. Computational modelling of the transport phenomena occurring during convective drying of prunes. J. Food Eng. 111, 279–288. https://doi.org/10.1016/j.jfoodeng.2012.02.021.

Sajilata, M.G., Singhal, R.S., Kulkarni, P.R., 2006. Resistant starch - a review. Compr. Rev. Food Sci. Food Saf. 5, 1–17. https://doi.org/10.1111/j.1541-4337.2006.tb00076.x.

Sobral, P.J.A., Menegalli, F.C., Hubinger, M.D., Roques, M.A., 2001. Mechanical, water vapor barrier and thermal properties of gelatin based edible films. Food Hydrocolloids 15, 423–432. https://doi.org/10.1016/S0268-005X(01)00061-3.

Sun, M.L., Wu, D., Wang, M.Q., Jin, S.F., Wang, K.Z., 2011. Simulation analysis of fluid-structure interactions with moving mesh. Adv. Mater. Res. 305, 235–238. https://doi.org/10.4028/www.scientific.net/AMR.305.235.

Thakhiew, W., Waisayawan, P., Devahastin, S., 2011. Comparative evaluation of mathematical models for release of antioxidant from chitosan films prepared by different drying methods. Dry. Technol. 29, 1396–1403. https://doi.org/10.1080/07373937.2011.588816.

Us-Medina, U., Julio, L.M., Segura-Campos, M.R., Ixtaina, V.Y., Tomás, M.C., 2018. Development and characterization of spray-dried chia oil microcapsules using by-products from chia as wall material. Powder Technol. 334, 1–8. https://doi.org/10.1016/j.powtec.2018.04.060.

Valentas, K., Paul Singh, R., Rotstein, E., 1997. Handbook of Food Engineering Practice. CRC Press. https://doi.org/10.1201/9781420049077.

Wang, L., Sun, D.-W., 2003. Recent developments in numerical modelling of heating and cooling processes in the food industry—a review. Trends Food Sci. Technol. 14, 408–423. https://doi.org/10.1016/S0924-2244(03)00151-1.

Yu, F., Li, Z., Zhang, T., Wei, Y., Xue, Y., Xue, C., 2017. Influence of encapsulation techniques on the structure, physical properties, and thermal stability of fish oil microcapsules by spray drying. J. Food Process. Eng. 40, e12576. https://doi.org/10.1111/jfpe.12576.